OPTIMIZATION OF A HIGH EXPANSION ORC TURBINE USING A GENETIC ALGORITHM

Stephan H.H.J Smit[1*], Quirijn Eppinga[2], Gustavo J. Otero Rodriquez[1], Rene Pecnik[1]

[1] TU Delft, Process and Energy,
Delft, Zuid-Holland, The Netherlands
* Corresponding Author: (S.H.H.J.Smit@tudelft.nl)

[2] Triogen B.V.
Goor, Gelderland, The Netherlands
Contact Information (Quirijn.Eppinga@triogen.nl)

ABSTRACT

The expander of an organic Rankine cycle (ORC) is a critical component for the overall system performance. If a designer is able to increase the turbine efficiency by 10%, the overall cycle efficiency increases by 4%. However, methodologies and dimensionless diagrams used for steam and gas turbine design are unreliable for ORC turbines because of two reasons. First, the expansion process takes place in the dense gas region, where the ideal gas law equation is not valid. And secondly, the working fluid features a small enthalpy drop due to its molecular complexity, bringing about a large pressure ratio per turbine stage that, combined with the relative low speed of sound of the organic fluid, results in a highly supersonic flow in the stator outlet.

This work presents an aerodynamic optimization, by means of a genetic algorithm, of a cantilever rotor of a single stage high expansion (~100) ORC turbine, operating with toluene ($C_6H_5CH_3$) as a working fluid. The rotor blade geometry is defined by 18 geometrical parameters and is generated using an in-house blade design tool. The mechanical integrity of the blade geometry is assured by constraints on the minimal thickness of the blade. The resulting rotor geometry is evaluated using a Reynolds-averaged Navier-Stokes solver in a quasi-three-dimensional (Q-3D) framework to account for the increase of area over the rotor stage. A mixing-plane model connects the stator and rotor domains, making the simulation steady state. To model the non-ideal gas properties the EOS by Robinson et al. (1985) is used. The objective of the optimization is to minimize the total enthalpy at the outlet of the turbine stage.

The optimized geometry successfully reduces a large flow separation in the rotor blade suction side which was present in the original design. As a result, the entropy production is reduced and the total-to-static efficiency has increased by 4.3%. In the future the design will be manufactured providing the possibility of assessing the performance of the blade and the corresponding flow solution.

INTRODUCTION

In the past 50 years, the use of Organic Rankine (ORC) cycle-based systems to generate power from heat has steadily increased up till an estimated installed capacity of 2701 MW as of December 31st 2016 (Tartière and Astolfi, 2017). A major advantage of ORC's with respect to the traditional Rankine cycles, is the possibility of optimizing the cycle in terms of thermodynamic and techno-economic aspects by choosing different working fluids and expansion machines. Because of this potential for customization, ORC systems can be designed and optimized for a wide variety of heat sources. For instance they are used to convert waste heat from internal combustion engine exhaust, geothermal heat sources, biomass applications, solar thermal applications and many other (Alshammari et al., 2018). Furthermore, because of their low operational costs and small installation size they are very much suited for commercial use for low power applications (<10 MW) (Alshammari et al., 2018).

Designing a highly efficient turbine for ORC-applications is important because the overall cycle perfor-

mance is very sensitive to the efficiency of the turbine as the thermodynamic one is low due to the relative low temperature of the heat source. Traditional design methods for turbines are unsuited to design ORC turbines because they don't take into account the vapour properties of the working fluids. Close to the critical point, these properties deviate from the ideal gas properties and the speed of sound is much lower than for instance, steam or air (Colonna et al., 2015). This has large consequences for the design of the turbine (Colonna et al., 2008). Furthermore, because of the low speed of sound within the turbine, supersonic and/or transonic flow can be present. This results in shock waves within the machine that introduce significant additional losses, which should be accounted for in the design method.

One of the design methods for turbines that is capable of taken into account the complexities in designing ORC-turbines is the so-called shape optimization method. In this method the shape of a turbine, determined by a high dimensional parameter space, is optimized by means of an optimization algorithm where the performance of each design is evaluated by means of a Computational Fluid Dynamics (CFD) simulation. These methods can be further divided into two categories: the gradient-based and the stochastic design method.

In gradient-based design methods the optimal shape is found by using the gradients of the objective function (with respect to the design variables) to progress towards the optimal design. Because the design of turbomachinery often requires a large number of design parameters, the adjoint method is the most appropriate technique to determine the gradients in a cost effective manner (Peter and Dwight, 2010). This method is characterized by the relatively low number of steps necessary to reach a optimal design but is also prone to end up in a local optimum. Examples can be found in (Anand et al., 2018), (Pini et al., 2014), and (Vitale et al., 2017). This method is most suitable to find small shape changes with respect to an original design.

As an alternative to the gradient-based design techniques, stochastic methods are used for shape optimization algorithms. In particular Genetic Algorithms (GA) are often used as they are able optimize non-smooth objective functions, are easily constraint, and deal with multiple objectives without requiring any gradients (Reeves and Rowe, 2002). Because these algorithms sample a large part of the design space they are much less prone to end up in a local minimum. To reduce the inherent computational costs of the method, an approximate model is often used in the optimization procedure. In the work by Jubori et al. (2017a) this method has been used to perform a multi-objective optimization of a radial-inflow ORC-turbine, improving the power output of the initial design by 11.98%. Further examples can be found in (Jubori et al., 2017b), (Persico et al., 2018) and (Pasquale et al., 2013).. This method is most suitable to find new optimal shapes that deviate substantially from the original design.

In this work we will re-design a rotor for a single stage high expansion (~100) ORC turbine, operating with toluene ($C_6H_5CH_3$) as a working fluid. To determine the new rotor design, an aerodynamic optimization, by means of a GA, is performed, where a novel blade parameterization is used to generate rotor geometries. First, we will present the methodology, where the novel parameterization for a cantilever-type rotor is explained, the details of the CFD simulations and the chosen optimization strategy. Then, we discuss the outcome of the optimization procedure and compare the optimized shape with the original shape. And finally, a small discussion follows where we will reflect on possible improvements and future work.

METHODS

The method to determine the optimal blade shape for the investigated turbine will be presented in three parts: (1) the parameterization method of the blade shape, (2) the methods used to resolve the flow fields, and (3) the overall-optimization method for finding the optimal design.

Blade Shape Generator

The Blade Shape Generator (BSG) is a tool that can design a rotor blade for a cantilever-type turbine as a function of 18 parameters. In general, the design procedure can be summarized as follows: the blade shape is a consequence of a desired flow line that turns the flow as gradual as possible through the rotor-stage with an as gradual as possible area increase. The procedure, depicted in figure 1, consist of four steps: (1) a *flow line optimization* (2.1) where a desired flow line through the rotor stage is determined, (2) a *channel optimization* (2.1) that leads to a channel with an optimized width distribution through the rotor stage, (3) a *shroud optimization* (2.1) that results in a shroud distribution, and (4) the *tip construction* (2.1) that will construct the leading and trailing edge of the blade.

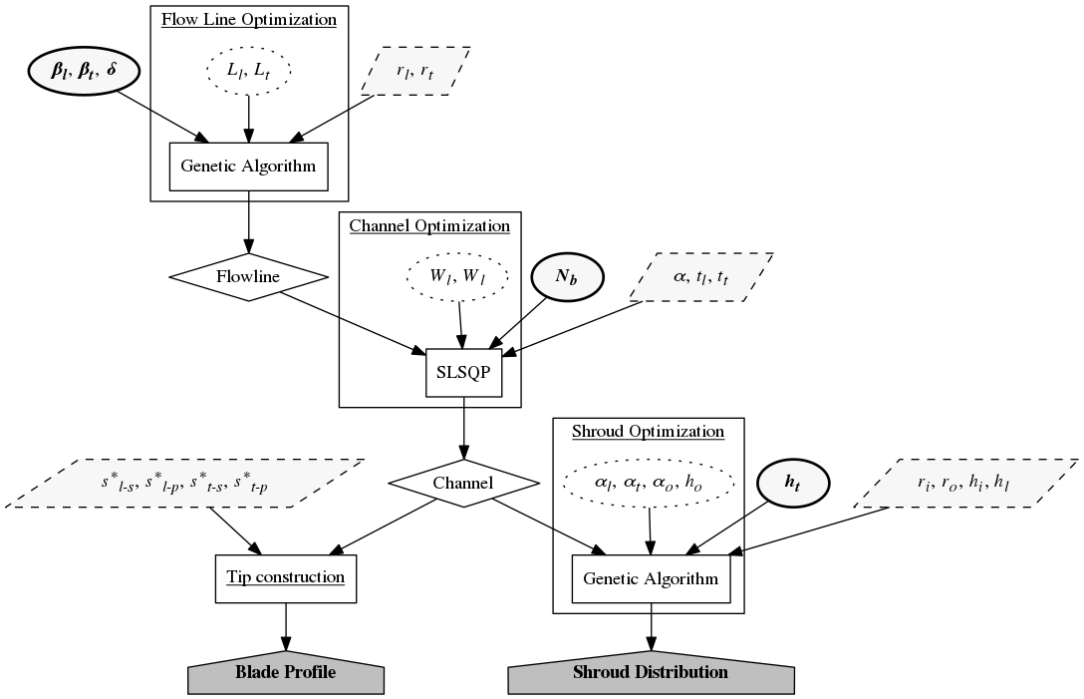

Figure 1: Schematic of the design procedure of the Blade Shape Generator (BSG), with the four steps underlined. In the bold ellipses the variables that will be optimized to find the best design, in the dotted ellipses the variables that will be optimized within the BSG, and in the dashed parallel-ograms the variables that are fixed. (See table 1a for the values).

Flow line optimization In the first step of the procedure a desired flow line through the rotor-stage is found by means of a genetic optimization. Five inputs are required: the radii of the leading and trailing edge (r_l, r_t), the angles of the flow line at those radii (β_l, β_t), and the stagger angle (δ) of the flow line. (See figure 1.) Given these parameters, the flow line is constructed by means of a Bezier curve with 2 control points. These control points are placed along two lines such that the inlet and outlet angle of the flow line are as specified. (See figure 2a.) What remains as free variables are the positions of the control points (L_l and L_t) along their corresponding line. These positions are found by solving the following minimization problem:

$$\begin{aligned} \min_{L_l, L_t} \quad & \sigma_f = \frac{1}{N}\sqrt{\sum_{i=1}^{N}\left(\left.\frac{d^2y_f}{dx_f^2}\right|_i - \overline{\frac{d^2y_f}{dx_f^2}}\right)^2} \\ \text{s.t.} \quad & r_t < r_{ctr,t} < r_{int}, \\ & r_{int} < r_{ctr,l} < r_l \end{aligned} \tag{1}$$

where y_f, and x_f are the coordinates of the flow-line, $r_{ctr,t}$ and $r_{ctr,l}$ the radii of the two control points, r_{int}

the radius where the two direction lines intersect, and N the number of discrete elements in the flow line. By minimizing the standard-deviation of the second derivative, a flow line is found that has a constant change of its first derivative, meaning the flow is turned as gradual as possible.

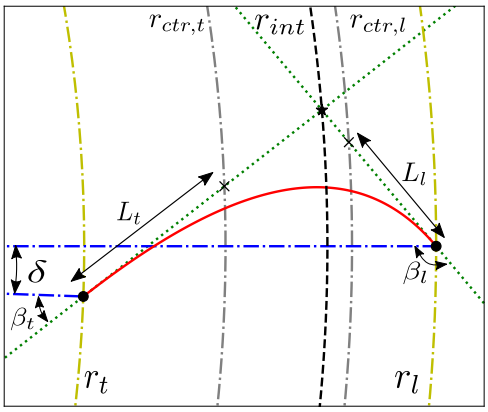

(a) The construction of the flow line depicted in red including the Bezier control points (×)

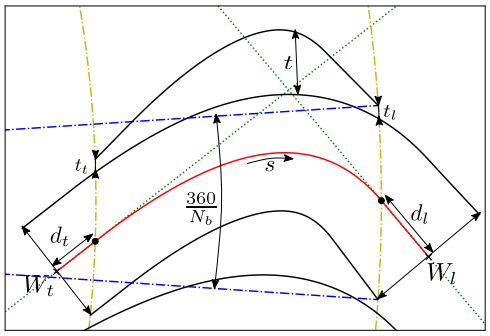

(b) The construction of the channel.

Figure 2: Blade parameterization in the $r\theta$-plane

Channel optimization The second step is to construct a channel by means of the flow line. An extended flow line will act as the channel center, and the width of the channel will be determined by means of an optimization procedure. Four inputs are required: the desired thickness of the leading and trailing edge (t_l and t_t) , the exponent γ in the width distribution relation (equation 3), and the number of blades N_b. (See figure 1.) Given these inputs, the width of the channel at the trailing and leading edge (W_l and W_t) will be determined by solving the following minimization problem:

$$\begin{aligned} \min_{W_t, W_l} \quad & \varepsilon = (t(r_l) - t_l)^2 + (t(r_t) - t_t)^2 \\ \text{s.t.} \quad & 1 < W_t < \infty, \\ & 1 < W_l < \infty \end{aligned} \tag{2}$$

where the width of the channel, W, as a function of distance s along the flow line is given by:

$$W(s) = \frac{W_l - W_t}{l^\gamma} s^\gamma + W_t. \tag{3}$$

The required extension distances d_l and d_t (see figure 2b) are determined with another gradient-based optimization procedure ((Nelder and Mead, 1965)) within the minimization problem given in equation 2. The thickness of the blade t, as a function of radius r, is calculated by rotating the bottom side of the channel upwards with an angle equal to $360/N_b$, and taking the difference between that rotated bottom and the top of the channel. (See figure 2b.) The solution to the minimization problem is found using a gradient-based optimizer ((Kraft, 1988)).

Shroud Optimization The third step is determining a shroud distribution for the rotor stage. Five inputs are required: the inlet and outlet radii (r_i and r_o), the inlet height, h_i, and the height of the blade at the leading and trailing edge (h_l and h_t). (See figure 1.) This leaves 4 variables free: the height and angle of the shroud line at the outlet (h_o and α_o), and the shroud angles at the leading and trailing edge of the blade (α_l, α_t). (See figure 3b.) These free variables are varied to solve the following minimization problem:

$$\begin{aligned} \min_{\alpha_l, \alpha_t, \alpha_o, h_o} \quad & \sigma_A = \frac{1}{N}\sqrt{\sum_{i=1}^{N}\left(\left.\frac{d^2A}{ds^2}\right|_i - \overline{\frac{d^2A}{ds^2}}\right)^2} \\ \text{s.t.} \quad & \alpha_l < 10, \\ & h_o > h_t \end{aligned} \tag{4}$$

where the area A at location i is given by:

$$A_i = \sum_{j=1}^{M} \frac{W_i}{M} h(r_{i,j}) \tag{5}$$

with h as the shroud height, M the number of discrete elements used to discretize the width of the channel at each location along the flow line, and N the number of discrete elements of the flow line. (See figure 3a.) By minimizing the standard deviation of the second derivative of the area distribution, a shroud distribution will be determined such that the area increase along the flow line will be as gradual as possible.

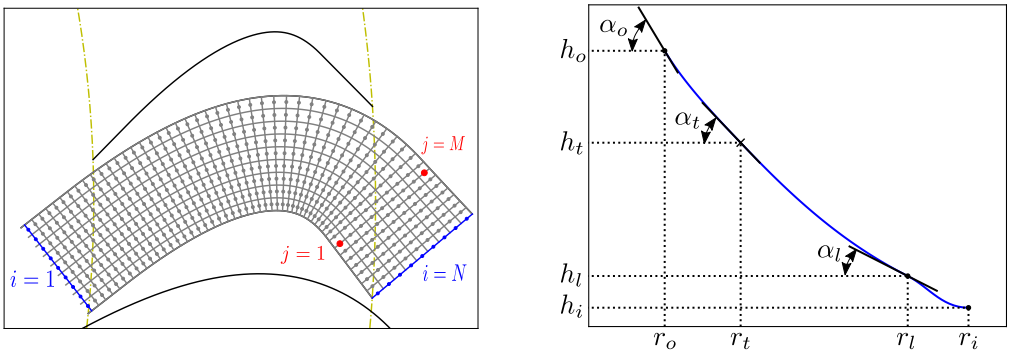

(a) The discretization of the channel **(b) The shroud parameterization.**

Figure 3: Example of an optimized channel

Tip construction The last and final step is the tip construction procedure. Four non-dimensional distances at suction and pressure side, for both the leading and trailing edge (s^*_{l-s}, s^*_{l-p} ,s^*_{t-s}, s^*_{t-p}), need to be specified. (See figure 1.) First, an approximate camber line is calculated by averaging the θ-coordinate of the top and bottom side of the blade, for each radius r. Second, to construct the trailing edge a normal line is drawn from this approximated camber line, to the suction side of the blade at non-dimensional position s^*_{t-s}, with the non-dimensional distance $s^* = \frac{s}{L}$, and L the length of the camber line. A spline will then be fitted through the intersection point (×) and the tip of the camber line. (See figure 4.) By specifying the derivatives at the start and end of this spline, the suction side will become continuous. Similar procedures are applied for the other edges. This will close the blade shape and ends the parameterization of the rotor.

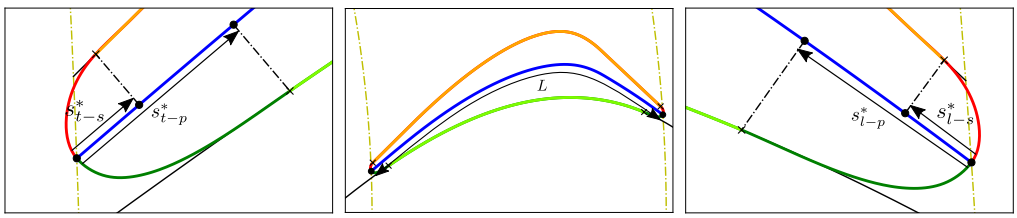

Figure 4: The construction of the leading and trailing edges: On the left the construction of the trailing edge using the non-dimensional distances s^* along the approximated camber line (depicted in blue), and on the right the construction of the leading edge.

CFD Simulation

Given the blade shape and the shroud constructed using the BSG, the flow fields for all the designs are resolved by means of CFD simulations using the open-source software SU2 (Palacios et al., 2013). To reduce computational complexity, each flow field is solved for a quasi-three-dimensional (Q3D) domain where the flow is solved along an assumed meridional line in the center of the shroud and the hub. This line is taken to be equal to half of the shroud height for each radius r. To account for the increase of area, the thickness of the mesh, as a function of the radius, is increased proportional to the shroud height.

To create the mesh for the different domains an in-house mesh tool is used. The stator domain is discretized with a structured mesh, including a boundary layer mesh. The boundary of the rotor blade is discretized using an O-mesh, but has an unstructured mesh for the rest of the domain, with two finer unstructured meshes at the leading and trailing edge. In the spanwise direction both of the meshes have three nodes. In the boundary layer mesh the first elements are clustered close to the wall to ensure that $y^+ \approx= 1$.

The following 4 boundary conditions are specified: (1) at the inlet, flow angle (α_1), total temperature and pressure (T_{01}, P_{01}), (2) at the outlet, static pressure (P_3), (3) between the stator and the rotor, a mixing plane model, and (4) for the top and bottom surfaces, symmetry conditions. (See table 1b for the corresponding values.) For all the surfaces, except the top and bottom, the non-reflecting boundary condition as presented by Giles (1990) is applied. To model the eddy viscosity the turbulence model of Spalart and Allmaras (1992) is used, the thermodynamic properties of toluene are calculated using the Equation of State (EOS) by Robinson et al. (1985) (with the critical pressure (P_c) and temperature (T_c)) and the transport properties, thermal conductivity (k) and viscosity (μ), are taken to be constant. (See table 1b for the values.) All equations are solved with a second order differentiation scheme, where limiters of Van Albada et al. (1997) and Venkatakrishnan (1995) are used for the momentum and turbulent equations respectively.

Optimization method

To obtain the optimal blade design, the following minimization problem is solved using a genetic algorithm:

$$\begin{aligned} \min_{\beta_l, \beta_t, \delta, N_b, h_l} \quad & h_{03} = f(\beta_l, \beta_t, \delta, N_b, h_l) \\ \text{s.t.} \quad & h_l < 30, \\ & N_b \in \{31, 37, 41, 43, 47, 53, 59\}, \end{aligned} \tag{6}$$

where f is the objective function to be optimized. This function consists of three steps: (1) the BSG that will create the blade profile and the shroud, (2) the transformation of the geometry into a Q3D mesh, and (3) solving the RANS equations using SU2. The final output of the function is the total enthalpy at the outlet of the rotor (h_{03}). (See figure 5.) To ensure fulfillment of the second constraint (equation (6)), the variable N_b will be set equal to the nearest number in the set.

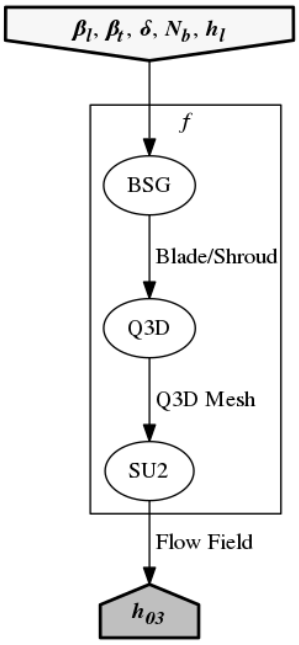

Figure 5: Diagram of the objective function *f*.

An initial population (n_{pop}) of 100 individuals is created and the algorithm is run for 10 generations (N_{gen} = 12). The mating and mutation probability (P_{mat}, P_{mut}) are taken to be equal to 0.9 and 0.02 respectively. To prevent duplicate individuals in the same generation, the mating and mutation strategy are adjusted such that only unique individuals will be created. To prevent individuals from being simulated twice, a list is kept of all the individuals that have been simulated, and if a new individual is created with the same genes, the fitness will be set equal to the already assessed individual. To scale the variables the following scaling is applied:

$$x^* = \frac{x - x_{min}}{x_{max} - x_{min}} \tag{7}$$

where x^* is the scaled variable. For the corresponding minima and maxima of the variables, see table 1c.

Table 1: Variables used in the optimization, where the subscript *orig* refers to the original geometry.

(a) BSG variables

	Parameter	Value	Units
BSG	r_l	r_{l-orig}	[mm]
	r_t	r_{t-orig}	[mm
	γ	1	[-]
	t_l	1	[mm]
	t_t	1	[mm]
	r_i	$r_{l-orig} \cdot 1.1$	[mm]
	r_o	$r_{t-orig} \cdot 0.8$	[mm]
	h_i	h_{i-orig}	[mm]
	h_l	h_{l-orig}	[mm]
	s^*_{l-s}	0.02	[-]
	s^*_{l-p}	0.05	[-]
	s^*_{t-s}	0.02	[-]
	s^*_{t-p}	0.05	[-]

(b) Q3D/SU2 variables

	Parameter	Value	Units
Q3D	r_3	r_{3-orig}	[mm]
	r_2	r_{2-orig}	[mm]
SU2	T_{01}	600-500	[K]
	P_{01}	3.3-2.9	[MPa]
	α_1	45	[°]
	P_3	0.01-0.1	[MPa]
	P_c	4.109	[MPa]
	T_c	591.79	[K]
	k	0.08029	[W m^{-1} K^{-1}]
	μ	18.53	[µPa s]

(c) GA variables

	Parameter	Value	Units
GA	N_{gen}	12	[#]
	n_{pop}	100	[#]
	P_{mat}	0.9	[-]
	P_{mut}	0.05	[-]
	$\beta_{l,min}$	$0.8 \cdot \beta_{l-orig}$	[°]
	$\beta_{l,max}$	$1.2 \cdot \beta_{l-orig}$	[°]
	$\beta_{t,min}$	$0.8 \cdot \beta_{t-orig}$	[°]
	$\beta_{t,max}$	$1.2 \cdot \beta_{t-orig}$	[°]
	δ_{min}	$0.1 \cdot \delta_{orig}$	[°]
	δ_{max}	$0.2 \cdot \delta_{orig}$	[°]
	$N_{b,min}$	$0.8 \cdot N_{b-orig}$	[#]
	$N_{b,max}$	$1.2 \cdot N_{b-orig}$	[#]
	$h_{t,min}$	$0.9 \cdot h_{t-orig}$	[mm]
	$h_{t,max}$	$1.1 \cdot h_{t-orig}$	[mm]

RESULTS

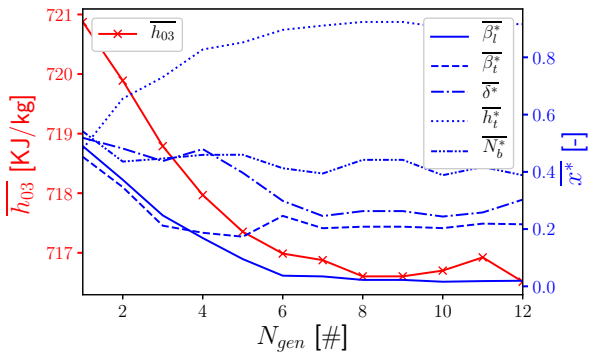

Figure 6: Mean total enthalpy per generation

Figure 6 shows the mean total enthalpy at the outlet of the turbine for different generations. It can be concluded that the optimization is progressing towards a minimum. The convergence of the optimization eems to be reached as the total enthalpy doesn't go down for the last numbers of generations. This indicates that the optimization reached convergence, however due to the stochastic nature of the optimization this is not garantueed. Furthermore, it also shows that in order to increase the power output of the turbine the height of the blade at the trailing edge (h_t) needs to be increased; i.e. the flow needs more area to expand.

Comparing the angles of the original and the optimized blade, we can observe that the optimized design has a higher leading angle (22.08%) but a smaller trailing and stagger angle than the original, -13.21% and -81.8% respectively.

In figure 7 the relative Mach number is plotted for the original, and the optimal design. In both cases the flow enters the rotor stage with a supersonic velocity in the relative frame of reference. One can observe the bow shocks at the leading edge of the rotor caused by the low rotational speed of the blade (Otero Rodriguez et al., 2019). In the case of the original geometry a large flow separation at the suction side of the blade is visible. In the optimized blade design, a much more gradual expansion is obtained, thereby reducing this separation bubble substantially, and in turn lessen the entropy generation in the rotor stage.

Table 2: Performance of new design with respect to original

	Difference	Units
$\Delta\eta_{t-t}$	2.296	[%]
$\Delta\eta_{t-s}$	4.368	[%]
Δp_{turb}	4.024	[kJ kg^{-1}]
ΔKE_3	-8.141	[kJ kg^{-1}]
ΔP_2	0.148	[bar]

Looking at the direction of the flow leaving the rotor stage we can observe that in the optimal design the relative outlet angle of the flow (in the θR-plane) has increased by 33.72%, this in turn leads to a lower

absolute outflow angle (≈ 0.3°) and thus less kinetic energy leaving the rotor. Furthermore, the mismatch between the relative flow angles and the blade angles are significantly reduced in the optimized design, meaning the blade is more in-line with the flow.

The power output of the optimized turbine has increased substantially with respect to the original, as can seen in table 2. The total-to-static efficiency has increased with 4.37% because of two reasons, (1) the reduction of kinetic energy leaving the turbine, and (2) less entropy generation due to the reduction of the separation wake. Furthermore, because of the increased thickness of the blade (i.e. a reduction of expansion area), the pressure at the interface of the rotor and the stator (P_2), has increased by 0.148 bar, leading to an increase of the degree of reaction of the turbine (4.31%).

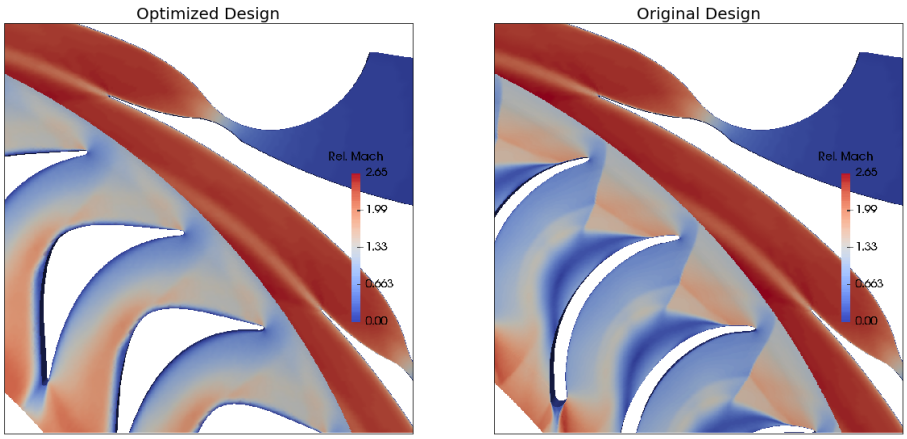

Figure 7: Relative Mach for the original design (left) and optimized design (right). (NB. Scaled for confidentiality.)

DISCUSSION

The optimization has lead to a new design that, according to the simulations, will improve the power output of the turbine considerably. However, because the flow is resolved in a Q3D manner, 3D flow effects are not accounted for. As is shown in the article by Otero Rodriguez et al. (2019) these effects can be substantial and the proposed increase of the shroud height can lead to extra losses due to separation at the shroud. Simulations and/or experimental data can help to quantify these effects in later studies.

Observing that the flow is still not completely in-line with the blade angles, it is expected that the optimal design presented in this study is not the global optimum and that optimizing for more generations and free parameters, will lead another design with a better performance.

We intend to improve the presented design method in the future. Envisioned adjustments are: (1) including real gas properties ((Lemmon and Span, 2006)) by means of table interpolation, (2) including a surrogate model to reduce computational costs, and (3) increase the design space by varying more parameters. The presented rotor design will also be manufactured so that the simulations can be validated with experimental data.

NOMENCLATURE

Symbol

α	Angle Shroud/Flow	(°)
β	Angle Flow Line	(°)
δ	Stagger Angle Flow Line	(°)
ε	Error	(-)
γ	Exponent in Channel Width Equation	(-)
μ	Viscosity	(µPa s)
A	Area of Channel	(mm^2)
f	Objective Function	($J\,kg^{-1}$)
h	Shroud Height/Enthalpy	(mm)
k	Thermal Conductivity	($W\,m^{-1}\,K^{-1}$)
l	Length of Camber Line	(mm)
L	Distance of control point	(mm)
N	Number	(#)
P	Pressure/Probability	(Pa/-)
p	Specific Power	(Pa/-)
r	Radius	(mm)
s	Distance along Camber Line/Flow Line	(mm)
T	Temperature	(K)
W	Width of Channel	(mm)
x	Carthesian coordinate on x-axis	(mm)
y	Carthesian coordinate on y-axis	(mm)

Subscript

0	Total Conditions
1	Inlet Stator
2	Interface Stator/Rotor
3	Outlet Rotor
b	Blades
ctrl	Control Point
f	Flow Line
gen	Generation
i	Inlet Shroud Line
l	Leading Edge
mat	Mating
max	Maximum
min	Minimum
mut	Mutation
o	Outlet Shroud Line
orig	Original
p	Pressure Side
pop	Population
s	Suction Side
t	Trailing Edge
turb	Turbine

Superscript

$*$	Non-Dimensional

REFERENCES

Alshammari, F., Usman, M., and Pesyridis, A. (2018). Expanders for organic rankine cycle technology. In *Organic Rankine Cycle Technology for Heat Recovery*. InTech.

Anand, N., Vitale, S., Pini, M., and Colonna, P. (2018). Assessment of ffd and cad-based shape parametrization methods for adjoint-based turbomachinery shape optimization. *Proceedings of Montreal*, 7:9th.

Colonna, P., Casati, E., Trapp, C., Mathijssen, T., Larjola, J., Turunen-Saaresti, T., and Uusitalo, A. (2015). Organic rankine cycle power systems: From the concept to current technology, applications, and an outlook to the future. *Journal of Engineering for Gas Turbines and Power*, 137(10):100801.

Colonna, P., Harinck, J., Rebay, S., and Guardone, A. (2008). Real-gas effects in organic rankine cycle turbine nozzles. *Journal of Propulsion and Power*, 24(2):282–294.

Giles, M. B. (1990). Nonreflecting boundary conditions for euler equation calculations. *AIAA Journal*, 28(12):2050–2058.

Jubori, A. A., Al-Dadah, R. K., Mahmoud, S., Ennil, A. B., and Rahbar, K. (2017a). Three dimensional optimization of small-scale axial turbine for low temperature heat source driven organic rankine cycle. *Energy Conversion and Management*, 133:411–426.

Jubori, A. M. A., Al-Dadah, R., and Mahmoud, S. (2017b). Performance enhancement of a small-scale organic rankine cycle radial-inflow turbine through multi-objective optimization algorithm. *Energy*, 131:297–311.

Kraft, D. (1988). A software package for sequential quadratic programming. *Forschungsbericht-Deutsche Forschungs- und Versuchsanstalt fur Luft- und Raumfahrt*.

Lemmon, E. W. and Span, R. (2006). Short fundamental equations of state for 20 industrial fluids. *Journal of Chemical & Engineering Data*, 51(3):785–850.

Nelder, J. A. and Mead, R. (1965). A simplex method for function minimization. *The Computer Journal*, 7(4):308–313.

Otero Rodriguez, G. J., Smit, S. H. H. J., and Pecnik, R. (2019). Three-Dimensional Unsteady Stator-Rotor Interactions in a High Expansion ORC Turbine. In *5th International Seminar on ORC Power Systems*.

Palacios, F., Alonso, J., Duraisamy, K., Colonno, M., Hicken, J., Aranake, A., Campos, A., Copeland, S., Economon, T., and Lonkar, A. (2013). Stanford university unstructured (su 2): an open-source integrated computational environment for multi-physics simulation and design. In *51st AIAA Aerospace Sciences Meeting including the New Horizons Forum and Aerospace Exposition*, page 287.

Pasquale, D., Ghidoni, A., and Rebay, S. (2013). Shape optimization of an organic rankine cycle radial turbine nozzle. *Journal of Engineering for Gas Turbines and Power*, 135(4):042308.

Persico, G., Romei, A., Dossena, V., and Gaetani, P. (2018). Impact of shape-optimization on the unsteady aerodynamics and performance of a centrifugal turbine for ORC applications. *Energy*, 165:2–11.

Peter, J. E. and Dwight, R. P. (2010). Numerical sensitivity analysis for aerodynamic optimization: A survey of approaches. *Computers & Fluids*, 39(3):373–391.

Pini, M., Persico, G., and Dossena, V. (2014). Robust adjoint-based shape optimization of supersonic turbomachinery cascades. In *Volume 2B: Turbomachinery*. ASME.

Reeves, C. and Rowe, J. E. (2002). *Genetic algorithms: principles and perspectives: a guide to GA theory*, volume 20. Springer Science & Business Media.

Robinson, D. B., Peng, D.-Y., and Chung, S. Y. K. (1985). The development of the peng-robinson equation and its application to phase equilibrium in a system containing methanol. *Fluid Phase Equilibria*, 24(1-2):25–41.

Spalart, P. and Allmaras, S. (1992). A one-equation turbulence model for aerodynamic flows. In *30th aerospace sciences meeting and exhibit*, page 439.

Tartière, T. and Astolfi, M. (2017). A World Overview of the Organic Rankine Cycle Market. *Energy Procedia*, 129:2–9.

Van Albada, G. D., Van Leer, B., and Roberts, W. (1997). A comparative study of computational methods in cosmic gas dynamics. In *Upwind and High-Resolution Schemes*, pages 95–103. Springer.

Venkatakrishnan, V. (1995). Convergence to steady state solutions of the euler equations on unstructured grids with limiters. *Journal of computational physics*, 118(1):120–130.

Vitale, S., Albring, T. A., Pini, M., Gauger, N. R., and Colonna, P. (2017). Fully turbulent discrete adjoint solver for non-ideal compressible flow applications. *Journal of the Global Power and Propulsion Society*, 1:Z1FVOI.

ACKNOWLEDGEMENT

The authors thank the Rijksdienst voor Ondernemend Nederland (RVO) who funded this research through the grant with project number TEHE116119.